Estuarine Exchange Flow Quantified with Isohaline Coordinates: Contrasting Long and Short Estuaries

SHIH-NAN CHEN

Institute of Oceanography, National Taiwan University, Taipei, Taiwan, and Applied Ocean Physics & Engineering, Woods Hole Oceanographic Institution, Woods Hole, Massachusetts

W. ROCKWELL GEYER AND DAVID K. RALSTON

Applied Ocean Physics & Engineering, Woods Hole Oceanographic Institution, Woods Hole, Massachusetts

JAMES A. LERCZAK

College of Oceanic and Atmospheric Sciences, Oregon State University, Corvallis, Oregon

(Manuscript received 29 April 2011, in final form 6 November 2011)

ABSTRACT

Isohaline coordinate analysis is used to compare the exchange flow in two contrasting estuaries, the long (with respect to tidal excursion) Hudson River and the short Merrimack River, using validated numerical models. The isohaline analysis averages fluxes in salinity space rather than in physical space, yielding the isohaline exchange flow that incorporates both subtidal and tidal fluxes and precisely satisfies the Knudsen relation. The isohaline analysis can be consistently applied to both subtidally and tidally dominated estuaries. In the Hudson, the isohaline exchange flow is similar to results from the Eulerian analysis, and the conventional estuarine theory can be used to quantify the salt transport based on scaling with the baroclinic pressure gradient. In the Merrimack, the isohaline exchange flow is much larger than the Eulerian quantity, indicating the dominance of tidal salt flux. The exchange flow does not scale with the baroclinic pressure gradient but rather with tidal volume flux. This tidal exchange is driven by tidal pumping due to the jet–sink flow at the mouth constriction, leading to a linear dependence of exchange flow on tidal volume flux. Finally, a tidal conversion parameter Q_{in}/Q_{prism}, measuring the fraction of tidal inflow Q_{prism} that is converted into net exchange Q_{in}, is proposed to characterize the exchange processes among different systems. It is found that the length scale ratio between tidal excursion and salinity intrusion provides a characteristic to distinguish estuarine regimes.

1. Introduction

The classic description of estuarine exchange flow is based on the tidally averaged longitudinal velocity at a fixed cross section (i.e., an Eulerian reference frame), which usually gives rise to a circulation with bottom inflow and surface outflow (e.g., Pritchard 1952). This circulation can largely be attributed to a baroclinic pressure gradient force set by a longitudinal density contrast (Pritchard 1956; Hansen and Rattray 1965), although a number of authors also invoke nonlinear tidal processes (e.g., Jay and Smith 1990a). The vertically and laterally sheared subtidal circulation transports salt up estuary, which balances the salt loss due to river and thereby maintains the salt content and longitudinal density gradient in estuaries (e.g., Chatwin 1976). The theoretical framework coupling the local momentum and salt balance with global salt budget is commonly noted in the literature (see review by MacCready and Geyer 2010) and has been successfully applied to understand the dynamics of long, partially mixed estuaries like the Hudson River, James River, and San Francisco Bay (Pritchard 1952; Geyer et al. 2000; Lerczak et al. 2006; Monismith et al. 2002).

The Eulerian analysis, however, reaches a limit when applied to short, salt-wedge types of estuaries such as the Merrimack (Ralston et al. 2010a), Columbia (Jay and

Corresponding author address: Shih-Nan Chen Institute of Oceanography, National Taiwan University, No. 1, Sec. 4, Roosevelt Road, Taipei 10617, Taiwan.
E-mail: schen77@ntu.edu.tw

DOI: 10.1175/JPO-D-11-086.1

Smith 1990b), and Connecticut (Garvine 1975) River estuaries. Some common features of these estuaries are that the river and tidal velocities are large and the salinity intrusion length scale is comparable to the tidal excursion. Large tidal variations of the structure of the salinity intrusion and the associated salt flux make the assumption of steady baroclinic pressure gradient in the traditional Eulerian analysis inappropriate for short, tidally variable estuaries.

When the Eulerian analysis is nevertheless applied to short estuaries, it has been found that the up-estuary salt transport by tidally averaged circulation does not balance the river-induced salt loss (e.g., Ralston et al. 2010a). Tidal processes instead provide the dominant up-estuary salt transport (e.g., Hughes and Rattray 1980). Many mechanisms have been proposed for this tidal salt flux, including oscillatory shear dispersion (Bowden 1965), tidal trapping (Okubo 1973), tidal pumping (Dronkers and van de Kreeke 1986; Stommel and Farmer 1952), and chaotic stirring (Zimmerman 1986) [see Fischer et al. (1979) for a review and section 4 for discussion]. However, there is no robust theory yet to predict the effective dispersion coefficient for this tidal flux (MacCready 2007), because of the spatial and temporal complexity of the tidal transport.

The general lack of predictive capability in tidal salt flux prompts estuarine investigators to seek alternative methods of quantifying salt flux that can be consistently applied to various estuaries. Recently, MacCready (2011) used an isohaline coordinate to calculate the subtidal estuarine exchange flow. As will be detailed in section 2, this method combines the subtidal and tidally induced transports, yielding inflow and outflow volume transport and salinity. These estuarine quantities [termed the total exchange flow (TEF)] exactly satisfy the Knudsen relation (Knudsen 1900; MacCready and Geyer 2010), irrespective of the fraction of salt transport accomplished by the tide. MacCready's (2011) analysis of the Columbia River salt flux showed that the exchange flow from the isohaline method was larger than that from Eulerian tidal averaging because the isohaline method explicitly accounts for tidal exchange processes. The exchange flow from the isohaline method decreased smoothly and monotonically with the distance from the mouth, whereas the Eulerian tidal averaging showed large fluctuations because of variations in the partitioning between tidal and residual flows. MacCready's analysis suggests that the isohaline method may provide a simpler and more robust mean of quantifying estuarine transport in highly time-dependent regimes.

The primary objective of this work is to compare the isohaline and Eulerian tidal averaging methods in quantifying estuarine exchange flow in different estuarine regimes. We apply both methods to the numerical simulations of two contrasting estuaries: the Hudson and Merrimack Rivers. The Hudson has a salinity intrusion typically much longer than the tidal excursion, and its salt flux is dominated by steady (subtidal) exchange. The Merrimack, on the other hand, has a salinity intrusion comparable to the tidal excursion, and its salt flux is dominated by tidal exchange processes. We explore the spatial structure and the responses of exchange flow to varying river and tidal forcing under the isohaline framework. Mechanisms responsible for driving salt fluxes in these two contrasting systems are identified, and scaling laws for the exchange are examined. Finally, we propose an estuarine regime classification based on the isohaline quantities, and the processes that differentiate estuarine regimes are discussed.

2. Methods

a. Numerical model of the Hudson River estuary

A numerical model of the Hudson River estuary has been developed and validated against observations using the Regional Ocean Modeling System (ROMS) (Warner et al. 2005). The model grid covers the 250-km-long tidal river from the Battery to the Federal Dam in Troy, New York. The grid highly resolves the first 40 km of the domain with an along-channel grid spacing of 300 m. The grid spacing then increases linearly between 40 and 250 km. The across-channel spacing is about 100 m. There are 20 sigma layers in the vertical. The model forcing, parameters, and boundary conditions are identical to the setup in Scully et al. (2009). Spring–neap tidal forcing consists of only M2 and S2 constituents. Four river discharges of 150, 300, 600, and 1200 $m^3 s^{-1}$ are considered. The k–ε turbulence closure with a stability function of Kantha and Clayson (1994) is used, and the bottom roughness is set to 2 mm. The salinity intrusion length, defined here as where the 2-psu isohaline intersects the bottom, varies inversely with river discharge, but, over the range of forcing considered here, the salinity intrusion length (30–80 km) is always significantly longer than the tidal excursion (8–11 km) (Fig. 1). The fluxes presented here are calculated at cross sections aligned with the model grid.

b. Numerical model of the Merrimack River estuary

A numerical model of the Merrimack River estuary has been developed and validated against observations using the Finite Volume Coastal Ocean Model (FVCOM) (Ralston et al. 2010a). The FVCOM grid covers 25 km upriver from the mouth and extends 35 km offshore. The estuarine interior and river mouth are highly resolved,

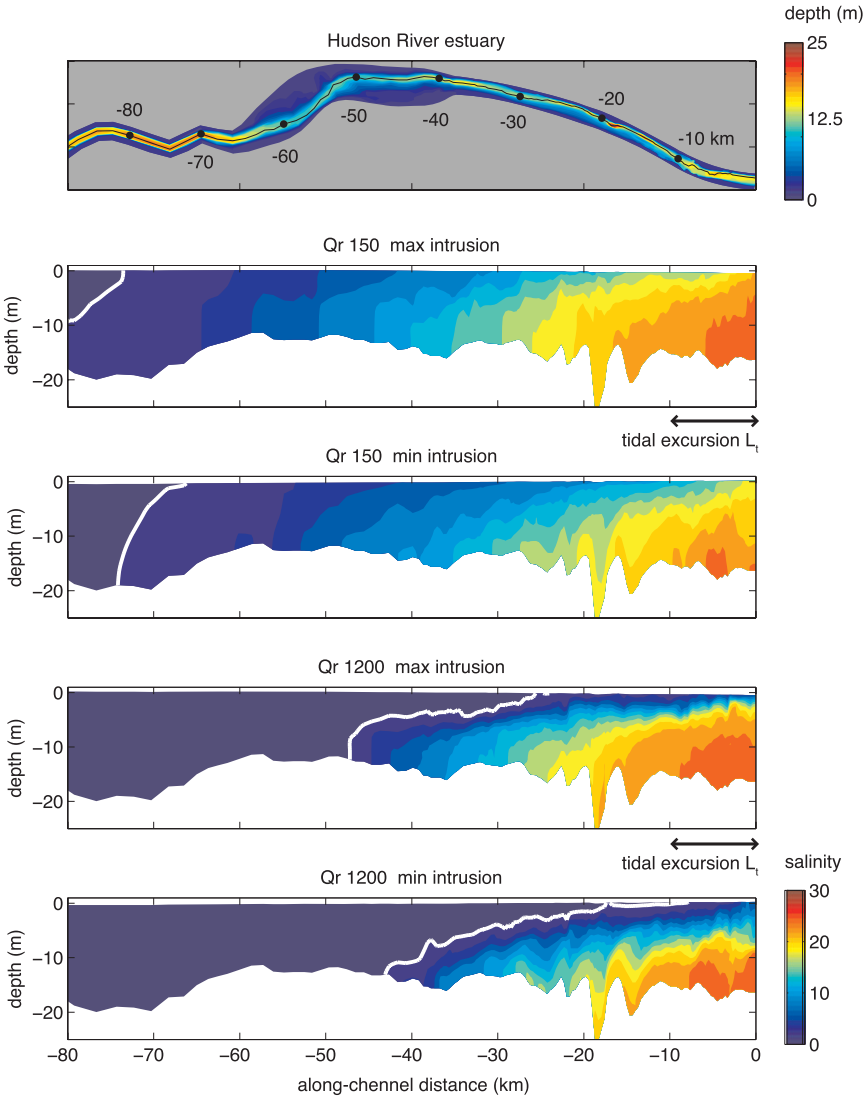

FIG. 1. (top) Hudson River model bathymetry and the spring–neap averaged along-channel salinity structures. Snapshots taken at (second row) maximum and (third row) minimum salt intrusion under low discharge condition (Q_r = 150 m^3 s^{-1}) and (fourth row),(bottom) under high discharge condition (Q_r = 1200 m^3 s^{-1}). The white contours indicate 2-psu isohaline. The black arrow denotes tidal excursion L_t for reference.

with grid spacing of about 20 m. There are 20 sigma levels in the vertical. The k–ε turbulence closure is used, with a constant bottom roughness of 5 mm. The calibrated model achieves a high skill score against the observation of water level, salinity, velocity, and salt fluxes (for details, see Ralston et al. 2010a). Numerical experiments with idealized M2 tidal forcing and constant river discharge were carried out for tidal ranges (2.0, 2.4, 2.8, and 3.2 m) spanning the spring–neap variability and river discharges (25, 50, 100, 200, 400, 700, and 1000 m^3 s^{-1}) that cover the seasonal variability. For each of the 28 experiments, the model was run to an equilibrium salinity intrusion. In the Merrimack, the salinity intrusion length (7–20 km) is comparable to the tidal excursion (10–17 km) (Fig. 2). The fluxes are calculated at cross sections with an average along-channel spacing of 400 m.

c. *Description of estuarine dynamics under Eulerian and isohaline framework*

A primary goal of this work is to compare and to provide linkages between the traditional Eulerian tidal averaging and the alternative isohaline method proposed by MacCready (2011). Here we briefly summarize

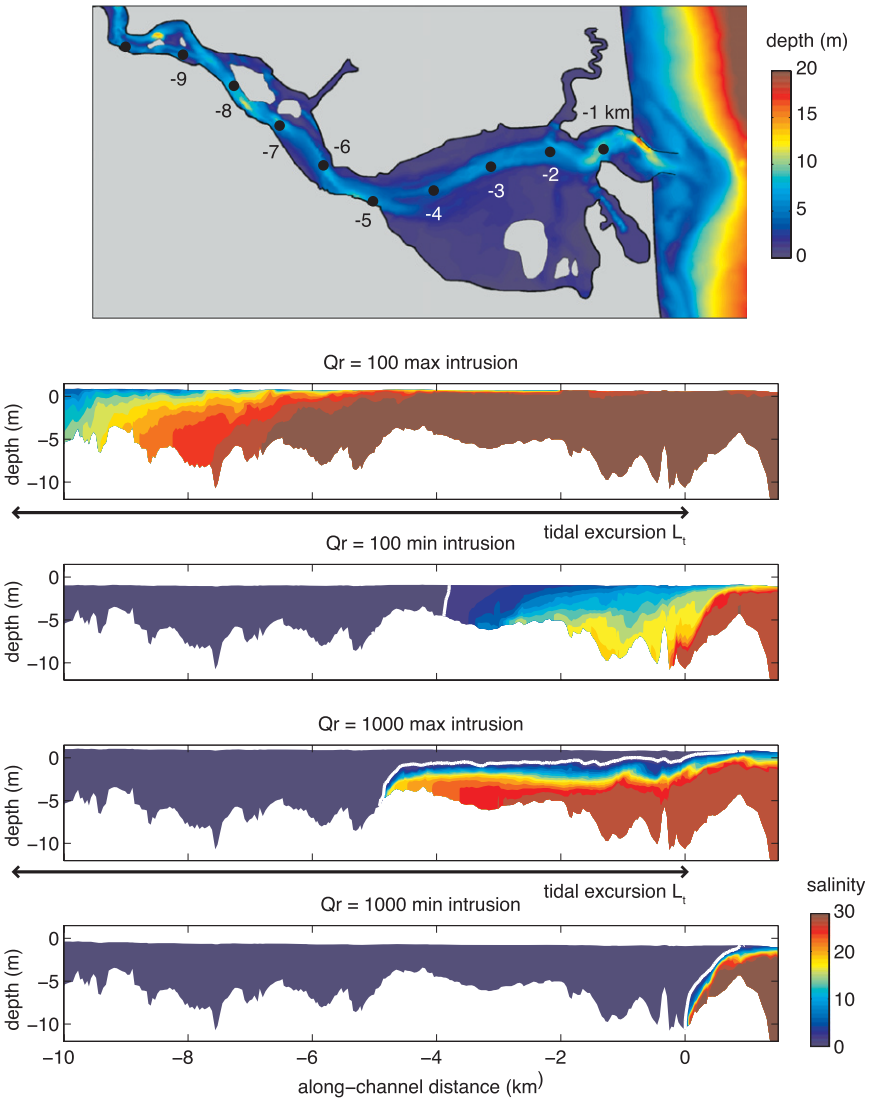

FIG. 2. (top) Merrimack River model bathymetry and the representative along-channel salinity structures with 2.4-m tidal range forcing. Snapshots taken at (second row) maximum and (third row) minimum salt intrusion under low discharge condition (Q_r = 100 m^3 s^{-1}) and (fourth row),(bottom) under high discharge condition (Q_r = 1000 m^3 s^{-1}). The white contours indicate 2-psu isohaline. The black arrow denotes the tidal excursion (L_t) for reference.

how the exchange flow, inflow–outflow salinity, and salt fluxes are obtained in each framework. Detailed definition of terms and derivations are given in MacCready (2011).

In the Eulerian framework, the longitudinal velocity u and salinity s at a channel cross section are decomposed into three orthogonal components: tidally and cross-sectionally averaged (u_0, s_0), tidally averaged and cross-sectionally varying (u_1, s_1), and tidally and cross-sectionally varying (u_2, s_2) values. For example, three velocity components are

$$u_0 \equiv \frac{\left\langle \int\int u\, dA \right\rangle}{A_0}$$
$$u_1(y,z) \equiv \frac{\langle udA \rangle}{\langle dA \rangle} - u_0$$
$$u_2(y,z,t) = u - u_0 - u_1, \qquad (1)$$

where the angel bracket represents tidal averaging, the area of integration A is divided into a constant number of differential elements dA that contract and

expand tidally, and $A_0 \equiv \langle \iint dA \rangle$ is the tidally averaged cross-sectional area. The Eulerian exchange flow refers to u_1. River discharge Q_r is equal to $-u_0 A_0$.

The subtidal total salt flux F can then be separated into three parts as

$$F = \left\langle \iint (u_0 + u_1 + u_2)(s_0 + s_1 + s_2)\, dA \right\rangle = \underbrace{-Q_r s_0}_{F_R} + \underbrace{\iint u_1 s_1\, dA}_{F_E} + \underbrace{\left\langle \iint u_2 s_2\, dA \right\rangle}_{F_T}, \quad (2)$$

where F_R indicates salt loss due to river, F_E is up-estuary salt flux driven by steady exchange flow (u_1), and F_T is the tidal salt flux. Although u_1, s_1, and therefore F_E may be estimated by an approximation of the subtidal momentum balance theories based upon Hansen and Rattray (1965) solution, the magnitude and spatial structure of F_T cannot be easily determined a priori. The relative contribution of F_E and F_T to up-estuary salt flux can be defined as $\nu^{\mathrm{Eu}} = [F_T/(F_E + F_T)]$ to classify steady-exchange-dominated (low ν^{Eu}) and tidal-exchange-dominated (high ν^{Eu}) estuaries (Hansen and Rattray 1966; superscript Eu indicates the calculation is in the Eulerian frame). However, ν^{Eu} cannot be determined with external variables (e.g., river and tidal velocities), again because of an inability to predict the tidal salt flux.

Assuming that exchange flow dominates the up-estuary salt flux ($F_E \gg F_T$) and applying the Hansen and Rattray (1965) solution for u_1 and s_1, the classic scaling laws for salt intrusion length L_s and exchange flow can be obtained as follows (Chatwin 1976; see also MacCready and Geyer 2010):

$$L_s \sim H c^{4/3} C_D^{-1} (u_0)^{-1/3} (U_t)^{-1}$$
$$u_1 \propto \frac{g\beta \partial s/\partial x H^2}{C_D U_t} = \mathrm{Si} U_t, \quad (3)$$

where U_t is the tidal velocity; $\partial s/\partial x$ is the longitudinal salinity gradient; H is the thalweg depth; C_D is the drag coefficient; β is the saline contraction coefficient; c is the speed of fastest internal wave ($c = \sqrt{g\beta s_0 H}$); and Si is the Simpson number, which represents the ratio of baroclinic forcing to bottom stress (Stacey et al. 2001; Burchard et al. 2011).

In the alternative isohaline framework, the subtidal exchange flow and salt flux are calculated by tidally averaging the transport as a function of salinity classes, rather than as a function of spatial position in a cross section. Following MacCready (2011), the tidally averaged volume transport through a cross section with salinity greater than s is defined as

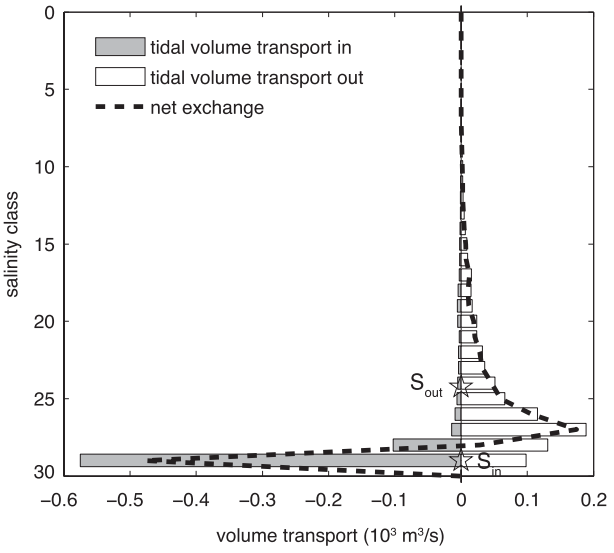

FIG. 3. Example of calculations of exchange flow and transport-weighted salinity. At a given cross section (Merrimack River mouth here), the volume transport is binned in terms of salinity classes (bin size is 1 psu). The white and gray bars are the outward and inward volume transport at a specific salinity bin over a tidal cycle. The net transport at a salinity class is then obtained by differencing the white and gray bars, denoted by the dashed line. The Q_{in} and Q_{out} are the summation of all inward (negative) and outward (positive) net transport, and S_{in} and S_{out} are the net-transport-weighted mean salinities, denoted by the star symbols.

$$Q(s) \equiv \left\langle \int\int_{As} u\, dA \right\rangle, \quad (4)$$

where As is the region of a cross section with salinity greater than s. Here, Q can be defined for all salinity $0 \le s \le s_{\mathrm{ocn}}$ (oceanic salinity set to 30 psu here). When integrating over all salinity classes, $Q(s = 0) = Q_r$. To find the tidally averaged volume transport at a specific salinity class, we differentiate Q with respect to salinity,

$$\frac{\partial Q}{\partial s} = \lim_{\delta s \to 0} \frac{Q(s + \delta s/2) - Q(s - \delta s/2)}{\delta s}. \quad (5)$$

Here, we use finite salinity bins with δs of 1 psu to create the function $\partial Q/\partial s$. Note that, if the fluxes in and out of a cross section at a salinity range δs are identical, then $\partial Q/\partial s$ is zero. MacCready (2011) gave an example that $\partial Q/\partial s = 0$ would occur for purely tidal advection of a "frozen" salinity field, as a water parcel is advected in and out of a cross section without being modified.

Taking a cross section near the Merrimack River mouth as an example, the white and gray bars in Fig. 3 represents the total outward and inward volume transport over a tidal cycle. The net flux δQ is the difference between white and gray bars for a specific salinity range

δs, as indicated by the dashed line [i.e., Eq. (5)]. Then, the exchange flow can be defined as

$$Q_{\text{in}} \equiv \int \frac{\partial Q}{\partial s}\bigg|_{\text{in}} ds, \quad Q_{\text{out}} \equiv \int \frac{\partial Q}{\partial s}\bigg|_{\text{out}} ds, \tag{6}$$

where Q_{in} and Q_{out} are the summations of negative (inward) and positive (outward) portions of the dashed line. Therefore, Q_{in} and Q_{out} represent the net transport of water into and out of the estuary because of both subtidal and tidal processes (MacCready 2011).

Salt fluxes and the transport-weighted salinities can be similarly defined as

$$F_{\text{in}} \equiv \int s \frac{\partial Q}{\partial s}\bigg|_{\text{in}} ds, \quad F_{\text{out}} \equiv \int s \frac{\partial Q}{\partial s}\bigg|_{\text{out}} ds$$
$$S_{\text{in}} \equiv \frac{F_{\text{in}}}{Q_{\text{in}}}, \quad S_{\text{out}} \equiv \frac{F_{\text{out}}}{Q_{\text{out}}}, \tag{7}$$

and the total volume and salt conservation are given by

$$Q_{\text{in}} + Q_{\text{out}} = -Q_r$$
$$\frac{d}{dt}\int\int\int s\, dV = Q_{\text{in}} S_{\text{in}} + Q_{\text{out}} S_{\text{out}}. \tag{8}$$

The isohaline framework gives a group of fundamental estuarine quantities, Q_{in}, Q_{out}, S_{in}, and S_{out}, which has been termed the total exchange flow by MacCready (2011). Under steady state, (8) becomes a generalized version of the Knudsen relation, $Q_r S_{\text{out}} = Q_{\text{in}} \Delta S$ ($\Delta S = S_{\text{in}} - S_{\text{out}}$). This generalized form of Knudsen relation differs from the conventional one by including the tidal fluxes. The isohaline method thus resolves the problem of undetermined tidal flux by combining subtidal and tidal processes into exchange flow Q_{in} and Q_{out}.

To make dynamically consistent comparison, we may use

$$Q^{\text{Eu}}(s) \equiv \left\langle \int\int_{\text{As}^{\text{Eu}}} (u_0 + u_1)\, \langle dA \rangle \right\rangle \tag{9}$$

to define similar tidally averaged quantities of $Q_{\text{in}}^{\text{Eu}}$, $Q_{\text{out}}^{\text{Eu}}$, $S_{\text{in}}^{\text{Eu}}$, and $S_{\text{out}}^{\text{Eu}}$ under the Eulerian framework (denoted by Eu superscript), as done in (6) and (7). Note that As^{Eu} is the region of a cross section with tidally averaged salinity ($s_0 + s_1$) greater than s. This means that only the subtidal components of the velocity ($u_0 + u_1$) and salinity ($s_0 + s_1$) are accounted. In the limit of zero tidal salt flux ($F_T = 0$), the exchange flow and inflow–outflow salinity quantified with two frameworks are identical. This suggests that, for steady-exchange-dominated systems (i.e., small F_T), we expect $Q_{\text{in}}^{\text{Eu}} \approx Q_{\text{in}}$ and $\Delta S^{\text{Eu}} \approx \Delta S$. In contrast, for tidal-exchange-dominated systems (i.e., large F_T), the tidal processes become important, and we anticipate much larger exchange flow calculated from the isohaline framework. Below, we use the Hudson and Merrimack River estuaries to examine these cases.

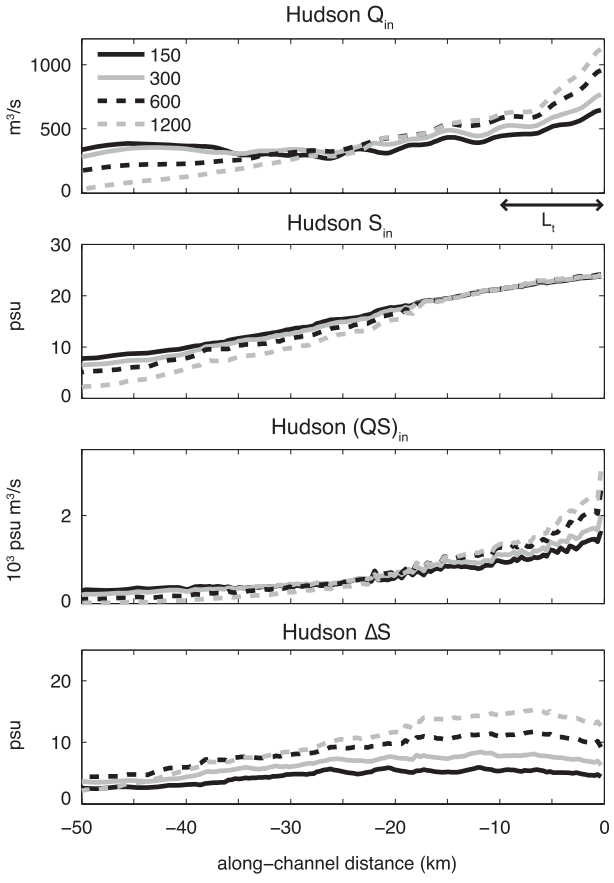

FIG. 4. Along-channel structures of (top) exchange flow Q_{in}, (second row) transport-weighted inflow salinity S_{in}, (third row) up-estuary salt flux $(QS)_{\text{in}}$ ($=Q_{\text{in}}S_{\text{in}}$), and inflow–outflow salinity difference ΔS in the Hudson River for all discharge conditions. These quantities are averaged over a spring–neap cycle.

3. Results

a. Hudson River exchange flow structure

Hudson River has an exchange flow that penetrates far landward from the mouth. In Fig. 4, we plot the exchange flow Q_{in}, transport-weighted inflow salinity S_{in}, up-estuary salt flux $(QS)_{\text{in}}$ ($=Q_{\text{in}}S_{\text{in}}$), and inflow–outflow salinity difference ΔS quantified using the isohaline method against the along-channel distance for four different discharge conditions. We average these quantities over a spring–neap cycle, because our intention is to evaluate the transport properties under a steady state and Hudson has a response time scale comparable to the spring–neap cycle during moderate discharge (Lerczak et al. 2009). As can be seen, Q_{in}, S_{in}, and up-estuary salt

flux all decrease smoothly landward, spanning a distance many times the tidal excursion. The isohaline framework provides a means of assessing the fluxes across isopycnals, based on conservation of salt and volume. The convergence of salt flux, $\partial(Q_{\rm in}S_{\rm in})/\partial x$, must be balanced by fluxes across the halocline (generally due to vertical salt flux), and the convergence of transport, $\partial Q_{\rm in}/\partial x$, must be balanced by cross-isopycnal entrainment. The gradual decrease of $Q_{\rm in}$ then indicates that most of the inflow continues to move landward without crossing the halocline and returned seaward. This is particularly pronounced during low-to-moderate discharge conditions (Q_r = 150 and 300 m^3 s^{-1}). The conveyer-belt-like exchange flow effectively transports salt landward, thereby maintaining a long salinity intrusion (e.g., Hunkins 1981). The salinity difference ΔS is relatively uniform along the estuary, and ΔS increases from roughly 3 to 11 psu as river discharge increases.

Although salt flux in the Hudson is dominated by steady exchange, the contribution of tidal salt flux is spatially variable and can be locally dominant. Taking Q_r of 300 m^3 s^{-1} as an example, the spatial mean of $\nu^{\rm Eu}$ is 0.2 (Fig. 5a). However, $\nu^{\rm Eu}$ at $x = -30$ to -50 km reaches around 0.4, and $\nu^{\rm Eu}$ can change abruptly in a short distance (e.g., from 0.4 to -0.4 between -15 and -18 km). The spatial variations of $\nu^{\rm Eu}$ reflect local changes in the partitioning between steady and tidal salt fluxes in the Eulerian framework. They are often associated with sharp bathymetric gradients. The locally elevated $\nu^{\rm Eu}$ at $x = -30$ to -50 km is associated with channel shoaling and expansion. The shallower water depth leads to a weaker Eulerian estuarine circulation and thus smaller steady salt flux F_E. Negative (counter gradient) tidal salt flux occurs at a deep hole and constriction around -18 km. The negative flux has been attributed to hydraulic response of the flow, with isohalines dipping down when the supercritical flood current passes through a bathymetric depression, which freshens the averaged salinity at this location and thus results in negative correlations between salinity and velocity (Engel 2009). However, when averaging over spatial variations, the tidal-salt-flux fraction $\nu^{\rm Eu}$ from the Eulerian decomposition is typically less than 25% of the total up-estuary salt flux within 50 km from the mouth, meaning that salt flux in the Hudson is dominated by steady exchange flow.

In the Hudson, the exchange flow and inflow–outflow salinity difference ΔS quantified with the isohaline method is largely consistent with the Eulerian analysis, except that it shows much less spatial variability than the Eulerian exchange flow $Q_{\rm in}^{\rm Eu}$. The variability of $Q_{\rm in}^{\rm Eu}$ is due to the varying partitioning between tidal and residual salt flux in an Eulerian reference frame, whereas

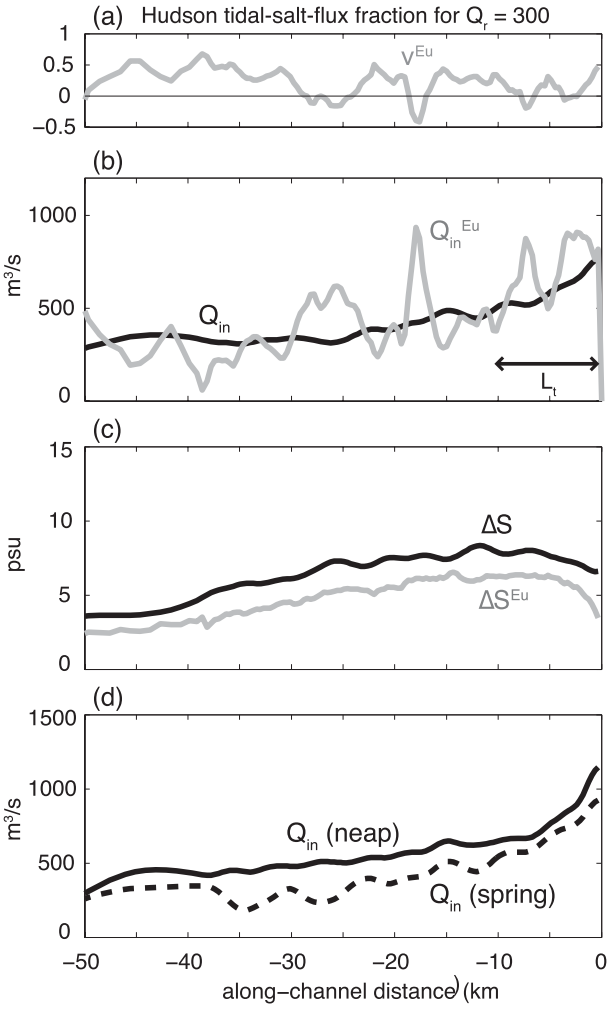

FIG. 5. Along-channel variations of (a) tidal-salt-flux fraction $\nu^{\rm Eu}$, (b) exchange flow $Q_{\rm in}$, (c) inflow–outflow salinity difference ΔS, and (d) exchange flow during spring and neap tides for the Hudson River. Case with discharge of 300 m^3 s^{-1} is taken as an example. In (a)–(c), the plotted quantities are averaged over a spring–neap cycle. In (b),(c), the exchange flow and ΔS quantified with isohaline (black lines) and Eulerian (gray lines) methods are compared. The Eulerian quantities are denoted by a superscript Eu.

the isohaline exchange flow $Q_{\rm in}$, varies smoothly, irrespective of local topographic variations (Fig. 5b). In the isohaline framework, ΔS shows the same spatial variations and has a similar magnitude as the Eulerian counterpart ($\Delta S - \Delta S^{\rm Eu} \approx 1$ psu). Furthermore, the exchange flow during neap tides is larger than that during spring tides (Fig. 5d), consistent with the observations by Geyer et al. (2000). These results indicate that the isohaline framework is generally consistent with the Eulerian analysis for the steady-exchange-dominated Hudson, but it does not exhibit the large-amplitude spatial variations in transport as suggested by the Eulerian approach.

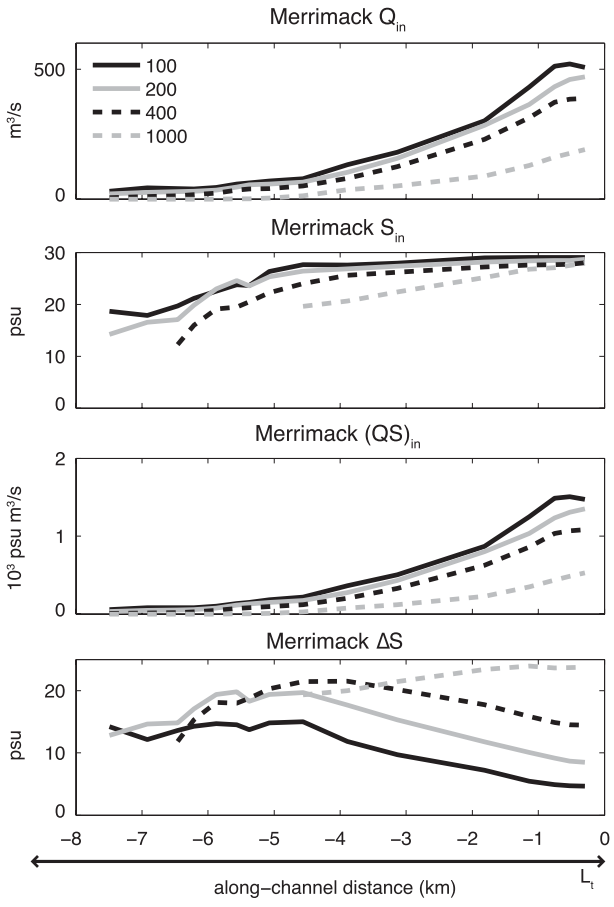

FIG. 6. As in Fig. 4, but for the Merrimack River under four discharge conditions. These quantities are averaged over four values of tidal forcing (2.0-, 2.4-, 2.8-, and 3.2-m tidal range) that bracket the range of spring–neap variability.

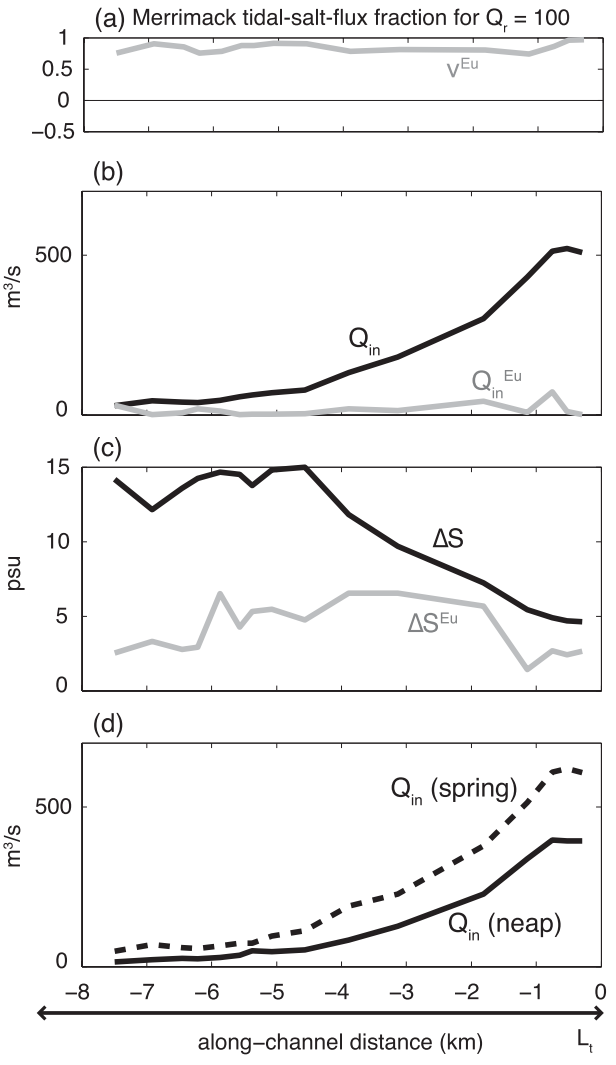

FIG. 7. As in Fig. 5, but for the Merrimack River, with the case with discharge of 100 $m^3 s^{-1}$ taken as a representative example. In (a)–(c), the plotted quantities are again averaged over four values of tidal forcing, as indicated in the caption of Fig. 6. In (d), only the cases with 2.0- (neap) and 3.2-m (spring) tidal forcing are plotted.

b. Merrimack River exchange flow structure

The Merrimack River estuary is very different from the Hudson River. The Merrimack is much shallower (average thalweg depth of 7 m, compared to 17 m in the Hudson), and the salinity intrusion is comparable to the tidal excursion. The isohaline exchange flow Q_{in} in the Merrimack again varies smoothly with along-channel distance (Fig. 6). In contrast to the Hudson, the magnitudes of Q_{in} and up-estuary salt flux $Q_{in}S_{in}$ decrease rapidly within one tidal excursion for a wide range of discharge conditions. This means that most of the net volume inflow crosses the isohaline surface to join the outflow within a short distance from the mouth (e.g., Ralston et al. 2010b). At the landward limit of the exchange flow, the inflow salinities S_{in} are equal to inflow–outflow salinity difference ΔS, consistent with a sharp salinity front at the head of the salinity intrusion (cf. Fig. 2). Throughout much of the estuarine domain, ΔS is greater than 10 psu. During moderate-to-high discharge conditions ($Q_r \geq 400$ $m^3 s^{-1}$), S_{in} and ΔS are similar in amplitude because the average outflow water is nearly fresh. The limited landward penetration of exchange flow and salt flux in the Merrimack sharply contrast the long, conveyer-belt-like Hudson.

The isohaline and Eulerian frameworks present strikingly different results for exchange flow and inflow–outflow salinity difference in the Merrimack. Taking the case with Q_r of 100 $m^3 s^{-1}$ as an example, the tidal-salt-flux fraction ν^{Eu} is high throughout the estuary (Fig. 7a). The spatial mean of ν^{Eu} is 0.84, indicating that the Merrimack River is a tidal-exchange-dominated system (e.g., Ralston et al. 2010a). The isohaline exchange flow Q_{in} and ΔS are much larger than Q_{in}^{Eu} and ΔS^{Eu} (Figs. 7b,c)

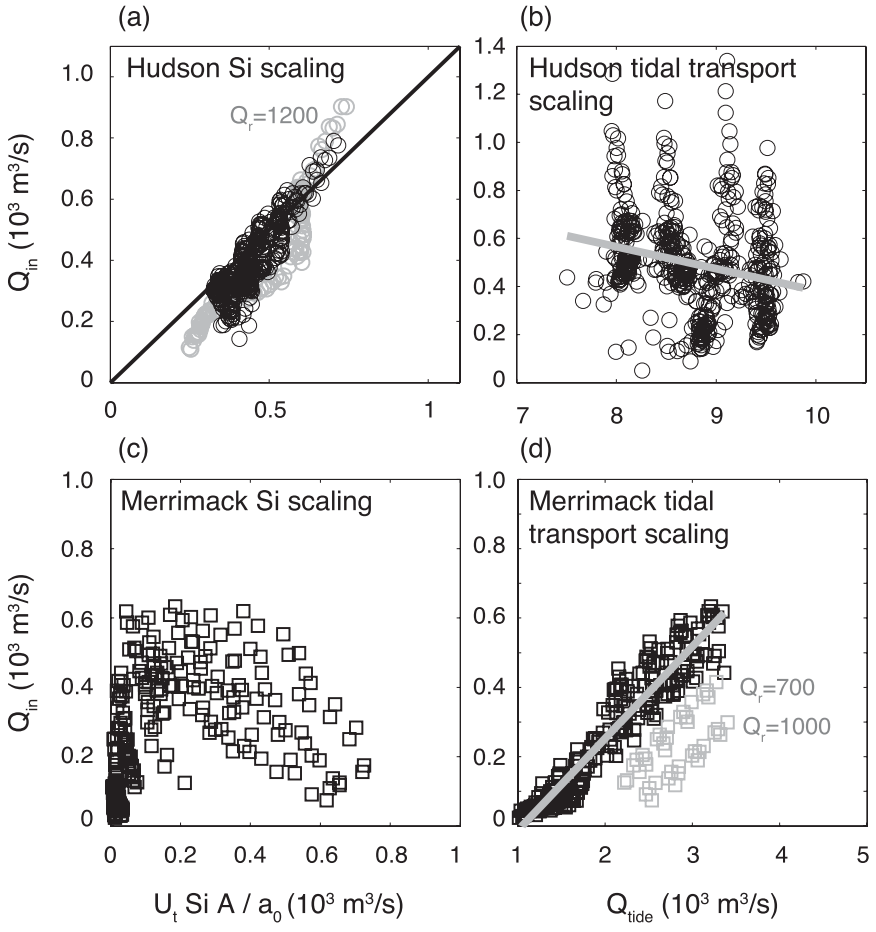

FIG. 8. Examination of scaling relation of the isohaline exchange flow for the (top) Hudson and (bottom) Merrimack Rivers. The magnitude of exchange flow is plotted against (left) the Si (Simpson number) scaling and (right) the amplitude of tidal volume flux Q_{tide}. (a) The highest discharge case is highlighted with gray circles. The black line indicates 1-to-1 relation. (b) The gray line is the linear regression (slope = -0.15, $R^2 = 0.22$). (d) Two highest discharge cases in which the influences of river flow on tides are significant are denoted by the gray squares. The gray line indicates the linear regression for low-to-moderate discharge ($Q_r \leq 400$ m^3 s^{-1}). The slope is 0.27, with R^2 of 0.91. In each panel, the complete set of idealized forcing experiments and transects with inflow salinity over 5 psu are plotted. An exception is the Hudson tidal transport scaling, for which only the discharge of 300 m^3 s^{-1} is plotted to illustrate spring–neap modulation.

because the isohaline exchange flow incorporates the tidal fluxes that are much greater than the steady fluxes.

Under uniform forcing conditions, the isohaline exchange flow varies with tidal amplitude, with greater exchange flow during spring tides than during neap tides (Fig. 7d). This positive correlation with tidal amplitude in the Merrimack contrasts the negative correlation in the Hudson, indicating major differences in salt flux mechanisms in these two systems.

c. *Parameter dependence and scaling laws of exchange flow*

In the previous sections, we have shown that the exchange flow and ΔS computed using isohaline coordinates are consistent with the Eulerian analysis in the Hudson River but are much larger than their Eulerian counterparts in the Merrimack River. We now examine the scaling of exchange flow obtained from isohaline method.

Two scaling relations are tested. First is a Simpson number *Si* scaling [i.e., Eq. (3)] that is based upon Hansen and Rattray's solution and attributes the exchange flow to the baroclinic pressure gradient ($\partial s/\partial x$). The second approach is a tidal transport scaling that relates exchange flow to the amplitude of tidal volume flux Q_{tide}, defined as the amplitude of $(\int\int u\,dA - u_0 A_0)$ to remove the offset by river flows.

In the Hudson, the exchange flow is found to correspond with the Si scaling (Fig. 8a). The exchange flow for

all discharge cases falls near the 1-to-1 line of $Q_{in} = U_t S i A/a_0$ (A is cross-sectional area and $a_0 = 8$ is a scaling factor), suggesting that the exchange flow in the Hudson is primarily driven by the baroclinic pressure gradient. Note, however, that the regression slope is slightly steeper than 1, especially for the higher discharge case (e.g., $Q_r = 1200$ m^3 s^{-1}; gray circle). As the discharge increases, the estuary shortens and the along-channel salinity gradient $\partial s/\partial x$ enhances. The slightly higher sensitivity of exchange flow on $\partial s/\partial x$ than the Si scaling can be explained by the increasing importance of tidal exchange processes as the estuary approaches the length of the tidal excursion. Scaling the exchange flow in the Hudson with tidal transport does not indicate a strong relationship (Fig. 8b). For example, at $Q_r = 300$ m^3 s^{-1}, the linear regression between Q_{in} and tidal volume flux is slightly negative (slope of -0.15), but the correlation is poor ($R^2 = 0.22$), with most of the variance coming from the spatial structure of Q_{in}. The slight decrease of exchange flow with increasing tides is consistent with Fig. 5d and with observations by Geyer et al. (2000) and is due in part to enhanced momentum transfer by tidal mixing.

Contrasting the Hudson, the Merrimack exchange flow does not correspond with the Si scaling (Fig. 8c), suggesting that the tidally averaged baroclinic pressure gradient is not the primary driving force for the exchange. Instead, the magnitude of exchange flow increases linearly with tidal transport (Fig. 8d). During low-to-moderate discharge conditions ($Q_r \leq 400$ m^3 s^{-1}; black squares), the tidal transport scaling produces an overall good linear fit ($R^2 = 0.91$; slope = 0.27). For two highest discharge cases ($Q_r = 700$ and 1000 m^3 s^{-1}; gray squares), this linear relation remains, but the magnitude of exchange flow falls below the linear regression line. This departure from a linear relation is explained by a reduction of tidal volume flux by strong river outflow (see section 4a for discussion). When the tidal transport scaling is applied to individual cross sections, the linear regressions yield R^2 between 0.90 and 0.99. The robustness of the tidal transport scaling suggests that tidal processes are largely responsible for driving the exchange flow in the Merrimack River.

4. Discussion

The above analysis suggests that the Hudson and Merrimack Rivers exhibit fundamentally different salt-flux mechanisms. In the Hudson, the salt flux is controlled by the density gradient (i.e., steady salt flux), and the exchange flow follows the conventional estuarine theory (i.e., Si scaling). In the Merrimack, the salt flux is controlled by tidal transport. However, mechanisms responsible for this tidal transport are not clear. Thus, in the discussion below, we first investigate the tidal salt flux mechanisms in the Merrimack. Then, in section 4b, we combine the findings from both systems into a regime classification.

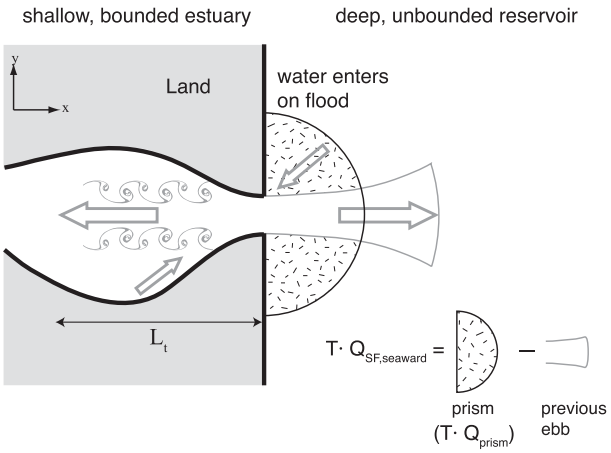

FIG. 9. Schematic of Stommel and Farmer's tidal pumping mechanism due to jet–sink flow structure at a river mouth constriction. The jet–sink exchange could occur on both sides of the mouth constriction. During one-half of the tide, water exits the constriction as a spreading jet, and, during the other half, the water enters the constriction as a radially symmetric sink flow. On the seaward side, with this idealized geometry, the volume of net exchange is the semicircular volume (i.e., tidal prism) minus the overlapping volume between inflow and outflow [see Eq. (10)]. On the landward side, the jet–sink exchange depends on interior bathymetry and is determined empirically [see Eq. (11) and section 4a for discussion].

a. *Tidal salt flux mechanisms in the Merrimack*

1) STOMMEL AND FARMER'S TIDAL PUMPING DUE TO JET–SINK FLOW

One potential tidal salt flux mechanism of relevance to the Merrimack is the tidal pumping due to jet–sink flow at a constriction, described by Stommel and Farmer (1952). The net salt transport results from tidal asymmetries in flow structure and properties (e.g., salinity). During one-half of the tide, water exits the constriction as a jet-like flow, and, during the other half, the water enters the constriction as a radially symmetric sink (Fig. 9). If the jet and sink flows have different salinity, then the asymmetry in flow structure leads to net salt transport. Note that the jet–sink exchange could occur concurrently on both sides of the constriction. In the case of the Merrimack, the exchange on the seaward side is more efficient, so the exchange processes on the landward side are more critical in limiting the overall tidal exchange (see below).

We apply the jet–sink flow scaling to the Merrimack River mouth and begin by describing the processes in the seaward region. Based on the flow geometry in Fig. 9 and assuming different salinity between inflow and outflow, the net inflow due to the jet–sink exchange may be expressed as

$$Q_{\mathrm{SF,seaward}} = Q_{\mathrm{prism}}\left[1 - \left(\frac{2}{\pi}\right)^{1/2}\left(\frac{B}{L_t}\right)^{1/2}\right], \quad (10)$$

where

$$Q_{\mathrm{prism}} = (Q_{\mathrm{tide}}/\pi) - (Q_r/2),$$

B is width of estuary mouth, L_t is tidal excursion, and Q_{tide} is the amplitude of tidal volume flux. The quantity $Q_{\mathrm{SF,seaward}}$ consists of two parts: Q_{prism} is the total volume of inflow in a tidal cycle (i.e., tidal prism; semicircle in Fig. 9) divided by the tidal period, and thus Q_{prism} represents the upper bound of exchange flow; the second part, $1 - (2/\pi)^{1/2}(B/L_t)^{1/2}$, is the exterior exchange ratio, which represents the fraction of inflow volume that is not coming from the reentry of precedent outflow jet. The exterior exchange therefore becomes more efficient as the mouth becomes narrower relative to the tidal excursion. Note that Q_{prism} in (10) includes a correction that accounts for the influences of river discharge on tidal volume flux. The correction becomes important during high discharge conditions when Q_{tide} and Q_r are comparable.

The estimate of net inflow in (10) is based on the original Stommel and Farmer theory applied to the seaward region of a river mouth (e.g., MacCready 2004). The key underlying assumption is that the salinity of the water drawn from the coastal ocean is completely transformed to lower-salinity classes inside the estuary. Such an assumption is not appropriate for the Merrimack because the jet–sink exchange processes also occur on the landward side of the mouth. During flood tides, oceanic water enters the estuary as a jet-like inflow that concentrates in the channel near the northern boundary (see below). Much of the ocean water is mixed to lower salinity classes during the time it spends inside the estuary, but some fraction returns to the coastal ocean unaltered. The return flow is evident in the seaward-directed volume flux of oceanic water (i.e., 30 psu salinity bin) in Fig. 3.

The scaling of jet–sink exchange flow occurring on both sides of the mouth constriction may be generalized as

$$Q_{\mathrm{SF}} = \alpha_{\mathrm{out}}\alpha_{\mathrm{in}}Q_{\mathrm{prism}}, \quad (11)$$

where α_{out} and α_{in} are the exterior and interior exchange ratio, respectively. In the Merrimack, α_{out} is roughly consistent with the idealization of jet and semicircular sink flow structure in Fig. 9 and may be estimated as $1 - (2/\pi)^{1/2}(B/L_t)^{1/2}$ [see Eq. (10)]. On the other hand, α_{in} cannot be readily evaluated because of the complex interior bathymetry, so α_{in} is determined empirically.

We find that the isohaline exchange flow in the Merrimack is consistent with the scaling of the generalized jet–sink exchange model [Eq. (11)]. In Fig. 10, the magnitude of exchange flow at the mouth for all of the idealized forcing experiments is plotted against Q_{prism}. The exterior exchange ratio α_{out} is estimated with the tidal-transport-weighted inflow salinity normalized by the ambient oceanic salinity, $\langle\int\int us|_{\mathrm{in}}\,dA\rangle / \langle s_{\mathrm{ocn}}\int\int u|_{\mathrm{in}}\,dA\rangle$, where $\langle\int\int us|_{\mathrm{in}}\,dA\rangle$ is the time-averaged salt flux into the estuary and $\langle\int\int u|_{\mathrm{in}}\,dA\rangle$ is the time-averaged volume transport (i.e., sum of gray bars in Fig. 3). Therefore, α_{out} represents the fraction of total tidal inflow that has oceanic salinity. This estimate of α_{out} yields values around 0.88–0.95 at the mouth, roughly consistent with the geometric estimate of 0.88 using Eq. (10) with the mouth width of 360 m and tidal excursion of 15 km. It is evident in Fig. 10 that, when only the exterior jet–sink exchange is considered, the model-derived exchange flow falls significantly below the scaling (gray shading; α_{out}= 0.88–0.95 and α_{in} = 1). Instead, the exchange flow is best described by the jet–sink flow scaling of

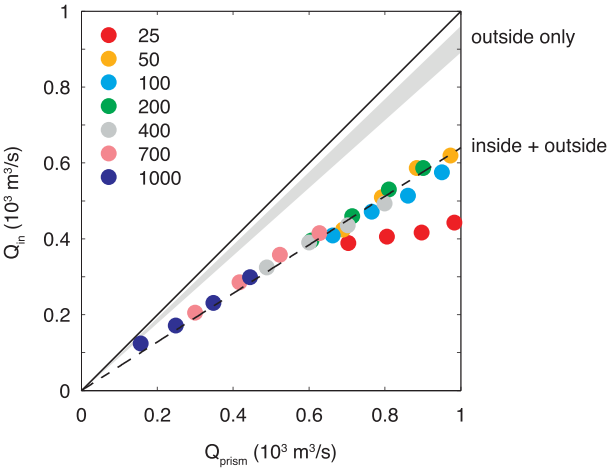

FIG. 10. The magnitude of exchange flow at the Merrimack River mouth for all of the idealized forcing experiments plotted against the tidal inflow rate Q_{prism}. Different color symbols denote different discharge conditions. The Merrimack exchange flow is best described by a generalized jet–sink exchange scaling of $Q_{\mathrm{SF}} = 0.65Q_{\mathrm{prism}}$, in which the exchange processes on both sides of the river mouth are considered [Eq. (11)]. The range of scaling for which only the exchange on the seaward side of the river mouth is considered is shown by the gray shading ($Q_{\mathrm{SF}} = 0.88 \sim 0.95\,Q_{\mathrm{prism}}$).

$$Q_{\mathrm{SF}} = 0.65Q_{\mathrm{prism}}, \quad (12)$$

which requires an interior exchange ratio α_{in} of 0.68–0.74. The high exterior exchange ratio α_{out} suggests that the tidal inflow is mainly consisted of the ambient, 30-psu oceanic water under the forcing conditions considered. The interior exchange is less efficient and is thus more critical in limiting the overall tidal exchange in the Merrimack.

The high discharge cases ($Q_r > 400$ m^3 s^{-1}) have weaker exchange flow than the low-to-moderate discharge cases

(Fig. 10). This is because the tidal inflow rate Q_{prism} is significantly reduced by the strong river flow. Note that the exchange flow of the lowest discharge case (Q_r = 25 m^3 s^{-1}) deviates from the jet–sink scaling of Eq. (12). In this case, the steady baroclinic exchange appears to contribute significantly to the salt transport, and the salinity intrusion becomes longer than the tidal excursion. The longer salinity intrusion reduces the salinity gradient available for mixing and thus leads to less effective conversion of tidal inflow into net exchange (see section 4b for discussion). Nevertheless, the correspondence between the isohaline exchange flow and the scaling of Eq. (12) suggest that the jet–sink mechanism at the mouth is likely responsible for driving the tidal exchange in the Merrimack.

The Eulerian decomposition of tidal salt flux also shows characteristics consistent with the jet–sink flow exchange. We decompose the Eulerian tidal salt flux term F_T in (2) into temporal and spatial components. The tidal velocity and salinity, u_2 and s_2, are sectionally averaged to find the temporal correlation $\overline{F_T} = \langle \int \overline{u_2 s_2}\, dA \rangle$ (i.e., barotropic tidal pumping). The correlation of the residuals gives the contribution due to spatial variations in velocity and salinity $F_{T,S} = \langle \int u_s' s_2'\, dA \rangle$, where $u_2'(y,z,t) = u_2 - \overline{u}_2(t)$ and the overbar is the section average. Taking the moderate discharge of 200 m^3 s^{-1} as an example, the temporal correlation $\overline{F_T}$ (blue dotted line) is largest at the mouth constriction (Figs. 11a–c). Moving landward, the estuary widens, and the contribution of spatial variations in velocity and salinity $F_{T,S}$ (black line) becomes dominant. The switch from temporal to spatial contribution of tidal salt flux is consistent with the jet–sink exchange. Away from the mouth, the inflow jet near the northern boundary generates marked lateral variations in velocity and salinity (Fig. 11b), but during the drainage-like outflow period the velocity and salinity structure is more laterally uniform. The tidal variations in velocity and salinity structure thus would lead to the elevated spatial contribution of tidal salt flux away from the mouth. Near the constriction, there is limited space for flow to exhibit spatial variability, and thus the tidal salt flux is dominated by temporal correlations $\overline{F_T}$. Note that $\overline{F_T}$ exhibits a secondary peak at another constriction near −5 km. This secondary peak is likely due to another jet–sink exchange. However, the exchange at this interior constriction is expected to be weaker relative to the mouth because the confined interior space limits lateral dispersion.

In the Merrimack, lateral variations in velocity and salinity dominate the spatial portion of the tidal salt flux $F_{T,S}$. Following Lerczak et al. (2006), the tidal salt flux due to lateral variations $F_{T,L}$ is estimated by vertically averaging u_s' and s_2' before integrating their product over the cross section. Similarly, the tidal salt flux due to vertical variations $F_{T,V}$ is obtained by laterally averaging prior to the integration. Note that, because the spatial decomposition is not orthogonal, the sum of the lateral and vertical components of flux will tend to exceed the total flux. However, such decomposition allows us to determine which component dominates. As Fig. 11d shows, the lateral contribution is about 3 times larger than the vertical contribution between the mouth and −5-km constrictions. The dominance of lateral contribution corresponds with the pronounced lateral variations in bottom salinity (Fig. 11b) and is consistent with the interior jet–sink structure.

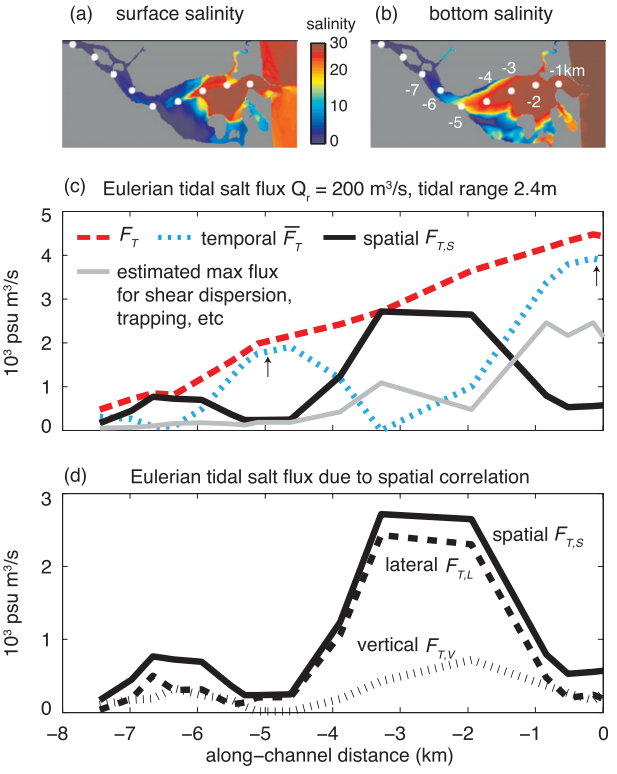

FIG. 11. Snapshots of (a) surface and (b) bottom salinity structures during midflood and (c),(d) the along-channel variations of tidal salt flux terms in the Merrimack River. The case with moderate discharge of 200 m^3 s^{-1} is taken as an example. In (c), the tidal salt flux F_T (red dashed line) is decomposed into contributions due to temporal (blue dotted line) and spatial (black) correlations. The gray line is the estimated maximum salt flux due to shear dispersion, tidal trapping, and chaotic stirring [see section 4a(2)]. The arrows indicate the location of the mouth and −5-km constrictions. In (d), the spatial correlation term shown in (c) is separated into lateral and vertical components. The sum of lateral and vertical components is not equal to the spatial correlation, because of the nonorthogonality [see section 4a(2)].

2) ESTIMATES OF TIDAL SALT FLUX DUE TO OTHER MECHANISMS

In addition to Stommel and Farmer's jet–sink exchange, other tidal dispersion mechanisms would be expected to

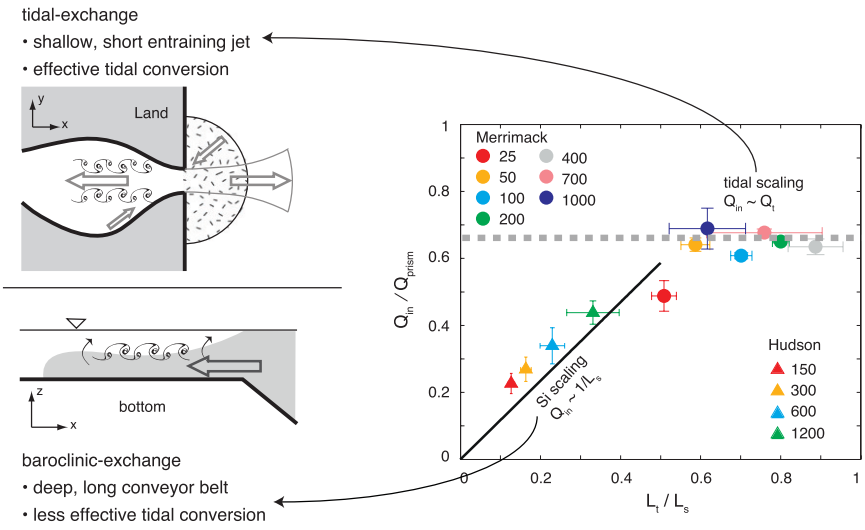

FIG. 12. Estuarine regime classification in terms of the tidal conversion ratio Q_{in}/Q_{prism} and the length scale ratio between tidal excursion and salinity intrusion L_t/L_s. The ratio Q_{in}/Q_{prism} measures the fraction of tidal inflow Q_{prism} (upper bound for exchange) that is transformed into net exchange Q_{in}. The Hudson and Merrimack results are denoted by triangles and circles, respectively. The Q_{in} at the mouth is used to indicate the magnitude of the exchange. Salinity of 2 psu near the bottom is used for computing salinity intrusion length L_s. Tidal excursion is calculated using the maximum depth-averaged tidal velocity in the thalweg at the mouth cross section. The error bars indicate spring–neap variability.

contribute to the salt transport. These mechanisms have been described in the literature as vertical and lateral shear dispersion (Bowden 1965), tidal trapping (Okubo 1973), and chaotic stirring (Zimmerman 1986). Despite a variety of parameterizations, these mechanisms essentially describe similar processes: they generally involve scalar advection by oscillatory flow, in combination with scalar displacement by mixing, trapping, or eddy stirring in the direction perpendicular to advection. These mechanisms are commonly parameterized in terms of a dispersion coefficient K. For all of these mechanisms, the maximum value of the dispersion coefficient occurs when the time scale of cross-sectional mixing matches the time scale of the tide, yielding an expression in the form

$$K_{\max} = \alpha U_t^2/\omega, \tag{13}$$

where ω is the tidal frequency. For vertical and lateral shear dispersion, the value of α depends on the flow structures and typically ranges from 0.005 to 0.02 in tidal estuarine environments (Fischer et al. 1979). For tidal trapping, the maximum α is around 0.05, with a trap–channel exchange time matching the tidal time scale and a trap–channel volume ratio ranging between 0 and 1 (Okubo 1973). For chaotic stirring, Zimmerman (1986) reported a maximum α is 0.05 for Dutch Wadden Sea.

We find that the tidal salt flux in the Merrimack significantly exceeds the maximum theoretical value that could be contributed by shear dispersion, trapping, or chaotic stirring. We use α of 0.05 as an upper bound for a dispersion coefficient with Eq. (13) and estimate the magnitude of tidal salt flux along the estuary with $AK\partial s/\partial x$, where A is the cross-sectional area and $\partial s/\partial x$ is the rms along-channel salinity gradient. Taking the moderate discharge condition as an example (Fig. 11c), the estimated upper bound of salt flux associated with shear dispersion, trapping, and chaotic stirring (gray line) is significantly below the model-derived value (red line). This result suggests that shear dispersion, tidal trapping, or chaotic stirring alone cannot account for the observed salt flux, consistent with the finding in section 4a(1) that the salt flux is dominated by the jet–sink exchange.

b. *Regime classification using isohaline analysis*

The Hudson and Merrimack represent different estuarine regimes, because they exhibit contrasting salt exchange mechanisms and salinity intrusion length scales. To characterize the relative magnitude of the exchange among different systems, we define a tidal conversion ratio Q_{in}/Q_{prism}, which measures the fraction of tidal inflow rate Q_{prism} [Eq. (10); upper bound for Q_{in}] that is transformed into net exchange Q_{in}. In Fig. 12, the tidal conversion ratio is plotted against the normalized length defined as the ratio of tidal excursion L_t to salinity intrusion L_s. The Q_{in} at the mouth is used to indicate the magnitude of the exchange.

The Hudson and Merrimack separate on the regime diagram: the Merrimack is characterized by short intrusion length and is effective in converting tidal inflow into net exchange (high Q_{in}/Q_{prism}), whereas the Hudson is characterized by a long intrusion length and has a lower tidal conversion ratio. In the Hudson, the salinity intrusion is much longer than the tidal excursion ($L_t/L_s \sim 0.12$–0.34). Less than half of the tidal inflow is transformed into net exchange ($Q_{in}/Q_{prism} \sim 0.20$–$0.45$). The exchange is mainly driven by the baroclinic pressure gradient (i.e., Si scaling), as indicated by the linear increase of the exchange flow with decreasing salinity intrusion for greater river discharge; In the Merrimack, the salinity intrusion and tidal excursion are comparable ($L_t/L_s \sim 0.5$–0.9). The conversion ratio is higher than the Hudson and is roughly constant [~ 0.65; Eq. (12)] over the all but the lowest discharge case. The exchange is driven by tidal pumping due to the jet–sink flow at the mouth constriction, leading to the linear dependence of exchange flow on tidal transport (i.e., constant Q_{in}/Q_{prism}) and the insensitivity to river discharge. For the lowest discharge case, there is some hint that the Merrimack is in transition between the tidal-exchange and baroclinic-exchange regimes, as shown by the dip down of Q_{in}/Q_{prism} for 25 $m^3\ s^{-1}$ discharge (see Fig. 10 and below).

The contrasting characteristics between these two systems may be understood in terms of the differences in length scale ratio L_t/L_s. Converting tidal inflow into net exchange requires mixing. In comparison with the Hudson, the Merrimack has a relative large length scale ratio, meaning that there are large salinity gradients available for mixing within the distance of one tidal excursion. However, the conversion of tidal volume flux to exchange flow and thus flushing in the Merrimack is limited only within one tidal excursion from the mouth (e.g., Fig. 6), because the inflow jet vigorously mixes with the estuarine water as it penetrates the estuary. In contrast, the longer Hudson has weaker salinity gradients and a lower tidal conversion ratio at the mouth. Note, however, that the baroclinic exchange in the Hudson extends multiple tidal excursions into the estuary. Even though the tidal conversion at the mouth of the Hudson is lower than the Merrimack, its overall effectiveness in horizontal salt transport is actually larger, based for example on an estuarine average effective dispersion coefficient.

The length scale ratio of L_t/L_s is governed by tidal and river forcing and water depth. Using Chatwin's (1976) theory to estimate the salinity intrusion length [Eq. (3)], we may write the length scale ratio as

$$\frac{L_t}{L_s} \sim \frac{2C_D}{\omega(g\beta s_0)^{2/3}} U_t^2 u_0^{1/3} H^{-5/3}. \tag{14}$$

The Chatwin scaling should be valid until L_s approaches L_t, at which point tidal processes would alter the scaling, but this parameter should effectively represent the decreasing significance of tidal processes as the ratio of L_t/L_s falls significantly below 1. Equation (14) states that, when tidal and river velocities increase, estuaries lose salt and decrease in length, whereas, for a deeper thalweg, the length of an estuary increases because of the enhancement of the baroclinic forcing. Rearranging (14) and using a transition criterion of $L_t/L_s \sim 0.5$ (Fig. 12), we obtain a critical depth that separates the baroclinic-exchange and tidal-exchange regimes,

$$H_c \sim \left[\frac{4C_D U_t^2 u_0^{1/3}}{\omega(g\beta s_0)^{2/3}}\right]^{3/5}. \tag{15}$$

Using a typical range freshwater velocity u_0 of 0.01–0.1 m s^{-1} and tidal velocity of 0.8–1 m s^{-1}, the critical depth is between 8 and 14 m. This range of critical depth falls between the baroclinic-exchange-dominated Hudson and the tidal-exchange-dominated Merrimack.

Although the proposed classification in Fig. 12 and the critical depth in Eq. (15) are able to distinguish between these estuaries, there are limitations and uncertainties that merit further investigations. For example, the estuarine characteristics for regime transition are unclear. Despite of the wide range of forcing considered, the Merrimack and Hudson do not overlap substantially in the proposed parameter space. The lowest discharge case of the Merrimack shows a tendency of transitioning toward the baroclinic-exchange regime, but the exchange flow still scales linearly with tidal volume transport (red circles in Fig. 10). The Columbia River has a length scale ratio located in the transition zone ($L_t/L_s \sim$ 0.4–0.7). However, MacCready (2011) reported a similar linear relation between the exchange flow and tidal strength. Thus, the location of the transition in L_t/L_s parameter space remains uncertain.

Furthermore, the regime diagram of Fig. 12 is constructed with exchange flow quantified at the mouth, based on observations that Q_{in} decreases landward smoothly from the mouth and therefore sets the exchange flow amplitude (e.g., Figs. 4, 6; MacCready 2011). For systems like fjords that have a deep main basin and a shallow sill at the mouth (e.g., large depth variations within one tidal excursion), Q_{in} at the mouth may not be representative of the overall properties. At a fjord's constricted mouth, tidal exchange may locally dominate over baroclinic exchange (e.g., Admiralty Inlet in Sutherland et al. 2011). However, the overall exchange characteristics may be set by density-driven flow in the main basin that composes the majority of fjord's

water volume. Similarly, caution should be used when applying the critical depth criterion of Eq. (15). The critical depth H_c is derived based upon Chatwin scaling for the salinity intrusion length. Chatwin's (1976) theory is valid for well-mixed and partially mixed systems where the exchange flow happens in the vertical dimension. The critical depth is not applicable to highly stratified estuaries like fjord and arrested salt wedge, where bottom-generated tidal mixing is dynamically less important. The critical depth may also be inappropriate for wide estuaries where the exchange occurs primarily in the lateral dimension, and vertical mixing does not play a key role in limiting the landward penetration of salt.

c. *Application of the isohaline analyses under realistic forcing*

The isohaline analyses can be extended to field data and numerical simulations with realistic forcing. To ensure adequate representation of volume and salt fluxes, field experiments that employ a dense cross-channel array of velocity and salinity measurement are desired. An alternative could be to use moored instruments in the channel and to carry out concurrent shipboard surveys for estimating cross-channel structures of velocity and salinity (e.g., MacDonald and Horner-Devine 2008). The isohaline method can be applied to field data or model results that contain multiple tidal frequencies by low-pass filtering the volume transport binned by salinity classes [i.e., replacing the tidal average in Eq. (4) with a tidal filter; MacCready 2011]. However, in tidal-exchange-dominated systems like the Merrimack, the linear relation between exchange flow and tidal volume transport is expected to be insensitive to the forcing frequencies, because the tidal strength is the primary controlling factor for the exchange. In baroclinic-dominated systems like the Hudson, the response of the exchange flow to tides likely will depend on the estuarine response time compared with the variability in the forcing (e.g., MacCready and Geyer 2010). When an estuary adjusts slower than changes in the forcing (e.g., the response time of the Hudson during low river discharge is longer than the spring–neap cycle), a negative relation between exchange flow and tidal transport is expected (e.g., Fig. 8b), and an averaging period longer than the characteristic forcing time scale is needed to ensure salt balance.

5. Conclusions

We have explored the spatial structures and parameter dependence of exchange flow in two contrasting estuaries, the Hudson and Merrimack Rivers, using validated numerical models under a wide range of idealized forcing conditions. Two methods for quantifying exchange flow are compared. First is the conventional Eulerian tidal averaging method that separates the tidal contributions to the flux from the Eulerian exchange flow. The alternative isohaline method, proposed by MacCready (2011), quantifies the exchange flow by averaging the transport in salinity space. The isohaline method yields an exchange flow that incorporates both subtidal and tidal fluxes into the total exchange flow and precisely satisfies the Knudsen relation.

We find that the isohaline method is a robust way to quantify exchange flow in different estuarine regimes. In the Hudson, the magnitudes and spatial structures of exchange flow and inflow–outflow salinity difference ΔS computed from the isohaline and Eulerian methods are similar, although the isohaline exchange flow is more spatially uniform. The isohaline exchange flow scales with the Simpson number Si, suggesting that the conventional Eulerian theory can be used to quantify the salt transport based on scaling with the baroclinic pressure gradient. In the Merrimack, on the contrary, the isohaline exchange flow and ΔS are much larger than the Eulerian counterparts, corresponding with the dominance of tidal salt flux. The isohaline exchange flow does not follow the Si scaling in the Merrimack but rather scales linearly with the tidal volume flux.

Mechanisms responsible for the tidal exchange in the Merrimack are investigated. We find that the exchange flow in the Merrimack is consistent with the scaling of Stommel and Farmer's jet–sink exchange mechanism after a modification to account for the exchange efficiencies on both sides of the river mouth constriction. Furthermore, the Eulerian decomposition of tidal salt flux shows alternations in partitioning between temporal and spatial correlations near the constriction, a pattern consistent with the jet–sink flow exchange. Other dispersive processes, such as shear dispersion, trapping, and chaotic stirring, are estimated to contribute at most 50% of the tidal salt flux. These analyses indicate that salt flux in the Merrimack is mainly controlled by tidal pumping due to the jet–sink flow at the mouth, consistent with the linear dependence of exchange flow on the tidal volume flux.

To characterize the relative magnitude of the exchange among different systems, we propose a tidal conversion ratio $Q_{\text{in}}/Q_{\text{prism}}$ which measures the fraction of tidal inflow Q_{prism} that is transformed into net exchange Q_{in}. An estuarine regime diagram is constructed, in terms of the tidal conversion ratio and the length scale ratio between tidal excursion and salinity intrusion L_t/L_s. The Merrimack is effective in converting tidal volume flux into net exchange, but the exchange is confined within one tidal excursion from the mouth. In contrast, the Hudson has a lower tidal conversion ratio, but the

baroclinic exchange extends multiple tidal excursions into the estuary. We suggest that the contrasting characteristics between these two regimes correspond with the differences in the length scale ratio L_t/L_s. This length scale ratio is sensitive to depth; thus, shallow estuaries are more likely to be dominated by tidal exchange flow and deep estuaries are more likely to be controlled by the strength of the baroclinic circulation.

Acknowledgments. SNC is supported by a WHOI postdoctoral scholarship, a NSF Grant OCE-0926427, and a Taiwan National Science Council Grant NSC 100-2199-M-002-028. WRG is supported by NSF Grant OCE-0926427. JAL is supported by NSF Grant OCE-0452054. SNC thanks Malcolm Scully for providing model results for the Hudson River and Parker MacCready for discussion on isohaline analysis.

REFERENCES

Bowden, K. F., 1965: Horizontal mixing in the sea due to a shearing current. *J. Fluid Mech.,* **21,** 83–95.

Burchard, H., R. D. Hetland, E. Schulz, and H. M. Schuttelaars, 2011: Drivers of residual estuarine circulation in tidally energetic estuaries: Straight and irrotational channels with parabolic cross section. *J. Phys. Oceanogr.,* **41,** 548–570.

Chatwin, P. C., 1976: Some remarks on the maintanance of the salinity distribution in estuaries. *Estuarine Coastal Mar. Sci.,* **4,** 555–566.

Dronkers, J., and J. van de Kreeke, 1986: Experimental determination of salt intrusion mechanisms in the Volkerak Estuary. *Neth. J. Sea Res.,* **20,** 1–19.

Engel, P. A., 2009: Spatial and temporal variability of tide-induced salt flux in a partially mixed estuary. M.S. thesis, Massachusetts Institute of Technology Dept. of Earth, Atmospheric, and Planetary Sciences and Massachusetts Institute of Technology/Woods Hole Oceanographic Institution Joint Program in Oceanography/Applied Ocean Science and Engineering, 45 pp.

Fischer, H. B., E. J. List, R. C. Y. Koh, J. Imberger, and N. A. Brooks, 1979: *Mixing in Inland and Coastal Waters*. Academic Press, 483 pp.

Garvine, R. W., 1975: The distribution of salinity and temperature in the Connecticut River estuary. *J. Geophys. Res.,* **80,** 1176–1183.

Geyer, W. R., J. H. Trowbridge, and M. M. Bowen, 2000: The dynamics of a partially mixed estuary. *J. Phys. Oceanogr.,* **30,** 2035–2048.

Hansen, D. V., and M. Rattray, 1965: Gravitational circulation in straits and estuaries. *J. Mar. Res.,* **23,** 104–122.

——, and ——, 1966: New dimensions in estuary classification. *Limnol. Oceanogr.,* **11,** 319.

Hughes, F. W., and M. Rattray, 1980: Salt flux and mixing in the Columbia River estuary. *Estuarine Coastal Mar. Sci.,* **10,** 479–493.

Hunkins, K., 1981: Salt dispersion in the Hudson estuary. *J. Phys. Oceanogr.,* **11,** 729–738.

Jay, D. A., and J. D. Smith, 1990a: Residual circulation in shallow estuaries 1. Highly stratified, narrow estuaries. *J. Geophys. Res.,* **95,** 711–731.

——, and ——, 1990b: Circulation, density distribution and neap-spring transitions in the Columbia River estuary. *Prog. Oceanogr.,* **25,** 81–112.

Kantha, L. H., and C. A. Clayson, 1994: An improved mixed layer model for geophysical applications. *J. Geophys. Res.,* **99,** 25 235–25 266.

Knudsen, M., 1900: Ein hydrographischer Lehrsatz. *Ann. Hydrogr. Marit. Meteor.,* **28,** 316–320.

Lerczak, J. A., W. R. Geyer, and R. J. Chant, 2006: Mechanisms driving the time-dependent salt flux in a partially stratified estuary. *J. Phys. Oceanogr.,* **36,** 2296–2311.

——, ——, and D. K. Ralston, 2009: The temporal response of the length of a partially stratified estuary to changes in river flow and tidal amplitude. *J. Phys. Oceanogr.,* **39,** 915–933.

MacCready, P., 2004: Toward a unified theory of tidally-averaged estuarine salinity structure. *Estuaries,* **27,** 561–570.

——, 2007: Estuarine adjustment. *J. Phys. Oceanogr.,* **37,** 2133–2145.

——, 2011: Calculating estuarine exchange flow using isohaline coordinates. *J. Phys. Oceanogr.,* **41,** 1116–1124.

——, and W. R. Geyer, 2010: Advances in estuarine physics. *Annu. Rev. Mater. Sci.,* **2,** 141–164.

MacDonald, D. G., and A. R. Horner-Devine, 2008: Temporal and spatial variability of vertical salt flux in a highly stratified estuary. *J. Geophys. Res.,* **113,** C09022, doi:10.1029/2007JC004620.

Monismith, S. G., W. Kimmerer, J. R. Burau, and M. T. Stacey, 2002: Structure and flow-induced variability of the subtidal salinity field in northern San Francisco Bay. *J. Phys. Oceanogr.,* **32,** 3003–3019.

Okubo, A., 1973: Effect of shoreline irregularities on streamwise dispersion in estuaries and other embayments. *Neth. J. Sea Res.,* **6,** 213–224.

Pritchard, D. W., 1952: Salinity distribution and circulation in the Chesapeake Bay estuarine system. *J. Mar. Res.,* **11,** 106–123.

——, 1956: The dynamic structure of a coastal plain estuary. *J. Mar. Res.,* **15,** 33–42.

Ralston, D. K., W. R. Geyer, and J. A. Lerczak, 2010a: Structure, variability, and salt flux in a strongly forced salt wedge estuary. *J. Geophys. Res.,* **115,** C06005, doi:10.1029/2009JC005806.

——, ——, ——, and M. E. Scully, 2010b: Turbulent mixing in a strongly forced salt wedge estuary. *J. Geophys. Res.,* **115,** C12024, doi:10.1029/2009JC006061.

Scully, M. E., W. R. Geyer, and J. A. Lerczak, 2009: The influence of lateral advection on the residual estuarine circulation: A numerical modeling study of the Hudson River estuary. *J. Phys. Oceanogr.,* **39,** 107–124.

Stacey, M. T., J. R. Burau, and S. G. Monismith, 2001: Creation of residual flows in a partially stratified estuary. *J. Geophys. Res.,* **106,** 17 013–17 037.

Stommel, H., and H. G. Farmer, 1952: On the nature of estuarine circulation. Woods Hole Oceanographic Institution Tech. Rep. 52-88, 131 pp.

Sutherland, D. A., P. MacCready, N. S. Banas, and L. F. Smedstad, 2011: A model study of the Salish Sea estuarine circulation. *J. Phys. Oceanogr.,* **41,** 1125–1143.

Warner, J. C., W. R. Geyer, and J. A. Lerczak, 2005: Numerical modeling of an estuary: A comprehensive skill assessment. *J. Geophys. Res.,* **110,** C05001, doi:10.1029/2004JC002691.

Zimmerman, J. T. F., 1986: The tidal whirlpool: A review of horizontal dispersion by tidal and residual currents. *Neth. J. Sea Res.,* **20,** 133–154.